Sources and trends of Black Carbon Aerosol in a Megacity of Nanjing, East China After the China Clean Action Plan and Three-Year Action Plan

Abudurexiati·Abulimiti [a,b], Yanlin Zhang [a,b], Mingyuan Yu [a,b], Yihang Hong [a,b], Yu-Chi Lin [a,b],*

Chaman Gul [c], Fang Cao [a,b]

[a] School of Ecology and Applied Meteorology, Nanjing University of Information Science and Technology, Nanjing, 210044, China

[b] Atmospheric Environmental Center, Joint Laboratory for International Cooperation on Climate and Environmental Change, Ministry of Education, Nanjing University of Information Science and Technology, Nanjing, 210044, China

[c] Reading Academy, Nanjing University of Information Science and Technology, Nanjing, Jiangsu, 210044, China

Correspondence to:

Yanlin Zhang* (zhangyanlin@nuist.edu.cn, dryanlinzhang@outlook.com)

Abstract Black carbon (BC) is an essential component of particulate matter (PM) with a significant impact on climate change. Few studies have investigated the long-term changes in BC and the sources, particularly considering primary emissions of BC, which is crucial for developing effective mitigation strategies. Here, three-year BC observations (2019-2021) were reported in Nanjing, a polluted city in Yangtze River Delta (YRD) region, eastern China. ~~Here, based on three-year observations (2019-2021), random forest (RF) algorithms were employed to reconstruct BC concentrations in Nanjing from 2014 to 2021. Source apportionment was conducted on the reconstructed data to investigate long-term trends of BC and its sources.~~ The results revealed ~~showed~~ that the ~~three-year~~ average BC concentration was 2.5±1.6 μg m^{-3}, peaking in winter, with approximately 80% attributed to liquid fuel combustion. Based on three-year monitoring data, the random forest (RF) algorithm was employed to reconstruct BC concentrations in Nanjing from 2014 to 2021. Source apportionment was conducted on the reconstructed time series, which revealed a significant decrease ($p < 0.05$) in BC levels over the eight-year period, primarily due to reduced emissions from liquid fuels. ~~Notably, the reconstructed time series revealed a significant decrease ($p < 0.05$) in BC levels over the eight-year period, primarily due to reduced emissions from liquid fuels. The comparison between two control polices periods (P1:2014-2017 and P2:2018-2021) indicate that BC~~

concentrations decline more steeply during S2 since significant ($p < 0.05$) reduction in biomass burning. Compared to the earlier control policy period (P1:2013-2017), BC concentrations declined more steeply after 2018 (P2) due to reduced solid fuel burning. The seasonal analysis showed indicated significant reductions ($p < 0.05$) in BC, BC_{liquid} (black carbon from liquid fuel combustion) and BC_{solid} (black carbon from solid fuel combustion) during winter, with BC_{liquid} accounting for 77% of the reduction. Overall, emission reduction was the dominant factor in lowering reducing BC levels, contributing between 62% and 86%, though meteorological conditions played an increasingly important role in P2, particularly for BC and BC_{liquid}. as revealed by Kolmogorov-Zurbenko (KZ) filter. However, during P2, meteorological conditions played a more significant role, especially in reducing BC and BC_{liquid}, with an increase in their impact on BC_{solid} compared to P1. Our results demonstrated that target control measures for liquid fuel combustion are necessary, as it liquid fuel combustion is a major driver of decreasing BC reduction, and highlight the non-negligible influence of meteorological factors over the long-term BC variations. especially in summer, while the influence of meteorological factors on BC variations cannot be overlooked.

Keywords: black carbon; sources; random forest; emission reduction

1. Introduction

Black carbon (BC), also known as element carbon (EC), is a carbonaceous component of particulate matter (PM) produced through incomplete combustion processes, including domestic cooking, heating and coke-making (Bond et al., 2013; Liu et al., 2020a). BC particles significantly influence the Earth's energy balance and are major contributors to global warming due to their strong absorption of solar radiation across visible to infrared wavelengths (Ramanathan and Carmichael, 2008; Ipcc, 2023). Additionally, the presence of BC particles in the atmosphere reduces atmospheric visibility and deteriorates air quality especially in urban areas due to their significant absorption properties (Ding et al., 2016). Exposure to BC aerosols has also been linked to increased health risks, such as heart attacks and cardiovascular diseases (Sarigiannis et al., 2015; Li et al., 2019). Owing to its short atmospheric lifetime of only 3 to 14 days, much shorter than that of greenhouse gases which can persist for decades, reducing BC

emissions can promptly mitigate global warming and benefit human health.

Accurate quantification of BC from different sources is essential to propose efficient mitigation strategies. Various methods in the past have been applied to BC source apportionment, including emission inventories (Zhu et al., 2020), radiocarbon isotope analysis (Zhang et al., 2014; Yu et al., 2023), and receptor models (Zong et al., 2016). However, uncertainties arise due to the lack of reliable emission factors, and receptor models require additional aerosol composition data. The radiocarbon source apportionment method is limited by its low temporal resolution, which hinders their ability to capture the dynamic changes in BC sources. In contrast, the Aethalometer model, with its high temporal resolution and rapid analysis, has been widely adopted for quantifying BC derived from liquid fuel (BC_{liquid}) and solid fuel (BC_{solid}) combustion (Lin et al., 2021; Sandradewi et al., 2008; Helin et al., 2018).

To address the sever air pollution issue, the Chinese government implemented the "China Clean Action Plan" during 2013-2017 and the "Three-Year Action Plan" during 2018-2020. Several studies in recent years have focused on long-term BC mass concentrations in major cities or regions of China to evaluate the impact of emission reduction measures implemented by the Chinese government (Sun et al., 2022a; He et al., 2023). However, while most of these studies document changes in BC concentrations, few have explored the specific contributions of different BC sources. Such an understanding is essential for identifying the drivers behind observed changes and for developing targeted mitigation strategies. Moreover, comprehensive datasets of BC are crucial for a better understanding of BC mass concentration variations and their implications for air quality policy. However, newly established monitoring stations often lack sufficient long-term observations, making it difficult to evaluate historical variations in BC concentrations. This limitation hinders efforts to understand BC dynamics in regions with limited prior monitoring, ultimately complicating the formulation of effective emission reduction policies. Chemical transport models (CTMs), which integrate meteorological conditions and emission inventories, are effective in simulating near-surface BC concentrations over short term periods (Cheng et al., 2019; Zhou et al., 2023). Nonetheless, their computational intensity and time-consuming often limit their application to long-term simulation. In contrast, the prediction of PM or other air pollutants can be efficiently

achieved through statistical models that establish relationships between measured values and various variables, including co-emitted pollutants, air humidity and air temperature. Recently, the historical values of nitrate $\delta^{15}N$ and $PM_{2.5}$ have been accurately reproduced based on the statistical relationships established between measured variables and other influencing factors (Fan et al., 2023; Zhao et al., 2020; Wu et al., 2024). This method provides a relatively straightforward approach for simulating historical air pollutants and is accurate enough for examining their long-term variations.

The long-term variation of atmospheric aerosol composition can be attributed to both ~~meteorology~~meteorological conditions and emissions. CTMs are one of the often used tools to quantify the impact of meteorology and emission on aerosols, as they consider the physical and chemical process that air pollutants undergo during their time in the atmosphere (Li et al., 2023; Zhang et al., 2019; Du et al., 2022). However, the accuracy of CTMs is often constrained by their initial conditions and uncertainty in emission inventory as well as models' underlying assumptions. Another commonly used method for separating the influences meteorology and emissions on target atmospheric pollutants is the Kolmogorov-Zurbenko (KZ) filter. For example, Sun et al. (2022b) found that meteorological contribution to the $PM_{2.5}$ trend presented a distinct spatial pattern over the Twain-Hu Basin, with northern positive rates up to 61% and southern negative rates down to -25%. Chen et al. (2019) reported that anthropogenic emissions contributed to 80% of reduction in $PM_{2.5}$ in Beijing from 2013 to 2017. Compared to CTMs, the KZ filter is easier to operate and is suitable for ~~any long~~long-term datasets of air pollutants, making it a practical tool for analyzing trends in atmospheric pollutants.

In the present study, a three-year BC mass concentration measurement was conducted to clarify BC characteristics and quantify contributions from different sources. The measured BC at two wavelengths (370nm and 880 nm) were used in ~~then incorporated into~~ random forest model to establish the nonlinear relationships with predictor variables, such as air pollutants and meteorological factors. Historical BC concentrations at the two wavelengths were reconstructed from 2014-2021 using the trained models to investigate the long-term temporal variation of BC and sources, with a focus on the two distinct emission reduction periods: the "China Clean Action Plan" and the

"Three-Year Action Plan". Finally, the impacts of meteorology and emissions on the long-term trend of BC were quantified to provide deeper insights into the factors driving its historical changes.

2. Data and Methods

2.1 Sampling site and Data

Nanjing is located eastern part of China, is vital industrial and economic center. The sampling instrument used for monitoring BC mass concentration was positioned on the rooftop of a seven-story building at the campus of Nanjing Information Science and Technology (NUSIT, 32.21°N, 118.72°E, Figure S1 in Supporting Information), Nanjing, China. The sampling site represents a typical urban ~~atmospheric environment~~atmosphere, encircled by local roads with an expressway approximately 1 km away. Moreover, a steel manufacturing plant and a petroleum chemical factory were about 5 km away from the sampling site. Traffic and industrial emissions are the primary sources of air pollution at the sampling site. Nanjing experiences four dominant seasons each year: winter (December-February), spring (March-May), summer (June-August), and autumn (September-November).

A dual-spot Aethalometer (AE33, Magee Scientific) was used to measure BC mass concentration from January 2019 to December 2021. The flow rate of AE33 was set to 5 L min^{-1} and the inlet cut-off size was 2.5 μm throughout the entire period. In brief, aerosol particles were collected on a filter tape automatically, and light attenuations (ATN) were measured at seven distinct spectral regions (370, 470, 520, 590, 660, 880, 950 nm) with a time resolution of 1 min. The ATNs were then converted to BC mass concentrations with seven different mass absorption cross sections (18.47, 14.54, 13.14, 11.58, 10.35, 7.77, 7.19 m^2 g^{-1}). In this study the BC concentration calculated by 880 nm spectral region was used, as BC is the predominant absorber at this wavelength (Drinovec et al., 2015). The BC data was missing since instrument maintenance from 13th July to 31st, 2020, and from July 23rd to September 26th, 2021. Hourly averaged concentrations of $PM_{2.5}$, CO, SO_2 and NO_2 were obtained from the China National Air Quality Monitoring Station, located approximately 10 km from the sampling site. Hourly resolution meteorological data, including temperature (T), relative humidity (RH), wind speed (WS), wind direction (WD) and boundary layer height (BLH), were sourced from the ERA5 reanalysis datasets provided by

176   the European Centre for Medium-Range Weather Forecasts (ECMWF).

177   **2.2 Aethalometer measurements and source apportionment**

178   The absorption Ångström exponent (AAE) describes the spectral

179   dependence of BC and is determined through a power-law fit between light

180   absorption ($b_{abs}(\lambda)$) and seven wavelengths, the equation can be written as:

$$b_{abs}(\lambda) = \beta \cdot \lambda^{-AAE} \tag{1}$$

181   where β is a constant dependent on aerosol mass concentration and size

182   distribution. Subsequently, the Aethalometer model is utilized to quantify the

183   contribution of liquid and solid fuels to BC. The model assumes that ambient

184   BC primarily originates from liquid fuel and solid fuel combustion, with BC

185   from two distinct combustion sources having differing light absorption

186   spectra. Hence, the total light absorption at 880 nm is attributed to liquid fuel-

187   generated BC (BC_{liquid}) and solid fuel-derived BC (BC_{solid}). The relationships

188   between $b_{abs}(\lambda)$, λ and AAE can thus be expressed as follows:

$$\frac{b_{abs}(\lambda_1)_{liquid}}{b_{abs}(\lambda_2)_{liquid}} = \left(\frac{\lambda_1}{\lambda_2}\right)^{-AAE_{liquid}} \tag{2}$$

189

$$\frac{b_{abs}(\lambda_1)_{solid}}{b_{abs}(\lambda_2)_{solid}} = \left(\frac{\lambda_1}{\lambda_2}\right)^{-AAE_{solid}} \tag{3}$$

190

$$b_{abs}(\lambda) = b_{abs}(\lambda)_{liquid} + b_{abs}(\lambda)_{solid} \tag{4}$$

191   where AAE_{liquid} and AAE_{soild} are the AAE values of BC from liquid and solid

192   fuel combustion, λ_1 and λ_2 are of different wavelengths. The selection of

193   wavelengths ~~(370-880 nm and 470-950 nm)~~ can impact source apportionment

194   results. <u>Considering brown carbon exhibits strong absorption at 370 nm and</u>

195   <u>that BC source apportionments at 470 and 950 nm are more consistent with</u>

196   <u>using radiocarbon techniques</u> (Zotter et al., 2017)<u>, the absorptions at 470 and</u>

197   <u>950 nm were ultimately chosen for source apportionment.</u> ~~Here, the 470 nm~~

198   ~~and 950 nm were chosen as they were recommended in the Aethalometer~~

199   ~~model (Drinovec et al., 2015).~~ Moreover, source apportionment result of the

200   Aethalometer model highly depend on selection of AAE pairs, with the value

201   of AAE being determined by the type of biomass, combustion processes and

202   long-ranged transport condition (Gul et al., 2021). The effect of different AAE

6

values on the results discussed in section 3.3.2 (source diagnostic tracer). Combining the equations (2) ~ (4), we can obtain the contribution of solid fuel combustion (BB%) to total BC:

$$BB(\%) = \frac{b_{abs}(\lambda_2)_{solid}}{b_{abs}(\lambda_2)} \times 100\% \tag{5}$$

Then, the BC$_{solid}$ can be obtained as follows:

$$BC_{solid} = BC(880nm) \times BB(\%) \tag{6}$$

Finally, the BC$_{liquid}$ can be calculated as:

$$BC_{liquid} = BC(880nm) - BC_{solid} \tag{7}$$

2.3 Building random forest model and tuning hyper parameters

The random forest (RF) machine learning algorithm is utilized to reproduce historical time series data of BC. RF, a model comprising hundreds of decision trees, splits data based on the informative features to avoid overfitting. However, decision trees can easily overfit, resulting in inaccurate model predictions. RF selects random samples of observation data for each decision tree, a common problem in decision trees, by using random data samples for each tree. The RF algorithm has been effectively applied in atmospheric chemistry studies ~~regions~~ for predicting PM$_{10}$ and organic carbon (OC) in different regions (Grange et al., 2018; Qin et al., 2022), demonstrating its strong predictive capabilities.

In this work, the BC concentrations from 2019-2021 (target variables) along with pollutant~~s~~ gases (SO$_2$, CO, NO$_2$) and meteorology factors such as T, RH, WS, WD and BLH (independent variables) were input~~ted~~ into the RF models. Although ~~–~~precipitation plays a key role in the wet scavenging of BC (Liu et al., 2020b; Ding et al., 2024), its inclusion in the RF model showed minimal contribution to predicting BC concentrations. The relatively lower contribution of precipitation can be attributed to the fact that its impact on BC typically appears over a longer time scale, while the model input is based on hourly precipitation, which may not adequately capture the cumulative effect. Furthermore, including precipitation in the model had no significant impact on its predictive performance; therefore, precipitation was excluded from the RF model. To train the RF model and assess the predictive ~~predicting~~ ability of ~~three~~ RF model~~s~~, the whole dataset was randomly divided into training and

testing sets in a ratio of 8:2. Given that observational data followed a log-normal distribution, most of the data are concentrated within a specific interval, resulting in~~a~~ poor model performance on extreme values. To ensure a good model performance, some data augmentation methods were used to achieve data balance by interpolating or duplicating ~~the~~ less frequent data, ensuring that the overall data~~set~~ roughly follows ~~essentially conforms to~~ a uniform distribution (Hong et al., 2023; Huang et al., 2023). To obtain optimal hyperparameter values, 10-fold cross-validation was utilized on the training sets, dividing the datasets into 10 subsamples, with ~~where~~ 9 subsamples ~~were~~ used for training ~~data~~ and 1 subsample for testing. The model performance of the 10-fold cross-validation is shown in Figure S2 and Figure S3. The results indicate that the RF-predicted BC at 880 nm correlated well with the observations, with an average R^2 of 0.97, MAE varying from 0.29 to 0.30, and RMSE ranging from 0.47 to 0.54. For BC at 370 nm, the cross-validation results were also robust, with a mean R^2 of 0.98, MAE values ranging from 0.37 to 0.41, and RMSE values varying from 0.57 to 0.74, confirming the stability and reliability of the model. Optimized parameters for the models were chosen based on the best mean squared error (~~MAE~~MSE), root mean squared error (RMSE) and R square (R^2) values obtained from the 10-fold cross-validation. Finally, the test sets were ~~then~~ input into the models and their predictive abilities were evaluated~~evaluated model predicting abilities~~. The optimized parameters selected for the models are presented in Table 1. The BC monitored by Aethalometer at 370 nm wavelength was also predicted by RF models with the same independent variables to explore ~~the~~ changes in BC sources in Nanjing from 2014 to 2021.

Table 1 Parameters used in random forest models

Parameters	Range	Optimal value	
		BC_880nm	BC_370nm
n_estimators	[100-350]	95	100
max_depth	[10-30]	25	23
max_feature	[auto, sqrt, log2]	sqrt	sqrt
criterion	[friedman_mse, poisson, squared_error, absolute_error]	absolute_error	absolute_error

2.4 Kolmogorov-Zurbenko filter

The KZ filter, a method for decomposing time series data into distinct

components, is widely utilized in air pollutants studies to differentiate the
influence of meteorology and emissions strength on the long-term trend of air
pollutants (Wise and Comrie, 2005; Yin et al., 2019; Chen et al., 2019). Since
the original concentration of BC follows a log-normal distribution, the data
(χ) were transformed into natural logarithmic form ($X = \ln (\chi)$) before
applying the KZ filter, allowing the data follow normally distribution (Zheng
et al., 2023). The KZ filter assumes that the original time series of a certain
air pollutant comprises short-term, seasonal, and long-term components. Thus,
the original time series of BC [X(t)] can be expressed as:

$$X(t) = E(t) + S(t) + W(t) \tag{8}$$

Here, E(t) represents the long-term component, mainly affected by climate,
long-range transport of air pollutants and emission intensity changes due to
shifts in energy structure. S(t) is the seasonal component, attributed to
variations in ~~meteorology~~meteorological conditions and emission intensity
across different seasons. W(t) is the short-term component driven by weather
patterns and fluctuations in local-scale emissions.

The KZ filter is a low-pass filter characterized by a window length (m)
and iterations (p). Different 'm' and 'p' values can be used to separate each
component of an air pollutant. $KZ_{(15,5)}$ can eliminate cycles that are less than
33 days and obtain the baseline component of the original data. The W(t) can
be easily obtained by subtracting $X_{BL}(t)$ from X(t). Therefore, the long-term,
short-term and seasonal components can be extracted as follows:

$$X_{BL}(t) = KZ_{(15,5)}[X(t)] = X(t) - W(t) \tag{9}$$

The X_{BL} is assumed to consist of its repeated climatological seasonal cycle
(X_{BL}^{clm}) and residuals (ε).

$$X_{BL} = X_{BL}^{clm}(t) + \varepsilon \tag{10}$$

The X_{BL}^{clm} contains most of the seasonality in X_{BL}, while ε consist of E(t) along
with minor seasonal variability unconsidered in X_{BL}^{clm}. Applying a KZ filter
with a window length of 365 and an iteration of 3 ($KZ_{(365,3)}$) to ε, the E(t) and
S(t) can be obtained:

$$E(t) = KZ_{(365,3)}[\varepsilon(t)] = X_{BL}(t) - S(t) \tag{11}$$

Due to emissions and meteorological condition changes can be both influence

on long-term trend of BC, the long-term component can be assumed to consist of emission-related (E_{LT}^{emi}) and meteorology-related (E_{LT}^{met}) components. Thus, the X_{BL} can be expressed as follows:

$$X_{BL}(t) = S(t) + E_{LT}^{emi} + E_{LT}^{met} \tag{12}$$

To derive the E_{LT}^{emi} in Eq._(9), the multiple linear regression model was ~~conducted~~ applied to the baseline component of BC and the ~~along with~~ baseline components of six meteorological factors including ~~such as~~ T, RH, WS, WD, BLH, surface pressure (SP). Then, the formulas can be written as follows:

$$X_{BL}(t) = a_0 + \sum_i a_i MET_{BL} + \varepsilon' \tag{13}$$

Where a_0 is the intercepts of multiple linear regression model outcomes. MET_{BL} denotes the baseline components of meteorology factors which are obtained by $KZ_{(15,5)}$. ε' is the sum of emission-related long-term variability and some minor seasonal variability unexplained by the multiple linear regression model. Therefore, the E_{LT}^{emi} can be extracted by applying $KZ_{(365,3)}$ to ε'. Then, the E_{LT}^{met} can be obtained by subtracting E_{LT}^{emi} from long-term component (E(t)) (Seo et al., 2018).

$$E_{LT}^{emi}(t) = KZ_{(365,3)}[\varepsilon'(t)] = E(t) - E_{LT}^{met}(t) \tag{14}$$

3 Results and Discussion

3.1 General characteristic of BC in Nanjing

Figure 1(a) shows the hourly (dots) and daily (line) mean variation of BC, $PM_{2.5}$ mass concentrations, and the proportion of BC to $PM_{2.5}$ in Nanjing. A 400-fold variation was found in hourly BC concentration, which ranged from 0.04 to 16.05 μg m^{-3}. Daily BC levels fluctuated much less than hourly concentration, from the lowest value of 0.40 μg m^{-3} (15th May 2021) to the highest value of 9.58 μg m^{-3} (24th January 2019). The average BC level during the whole sampling period was 2.52 ± 1.62 μg m^{-3}. Figure 1(b) illustrates the frequency distributions of hourly BC concentrations during different sampling periods. Over three years, BC distributions shifted toward lower values. In 2019, the most frequent BC concentrations were observed in 2 to 3 μg m^{-3} range, accounting for 26.2% of samples. In 2020 and 2021, the most BC levels were found in the 1 to 2 μg m^{-3} range, with frequencies of 38.0%

322 and 41.9%, respectively. BC levels exceeding 7 μg m^{-3} accounted for 5.1%,
323 0.8% and 0.01% in three years. PM$_{2.5}$ showed a similar variation to BC, with
324 a significant correlation (r = 0.74, p < 0.05) observed between daily PM$_{2.5}$ and
325 BC concentrations during sampling period. The hourly ratio of BC to PM$_{2.5}$
326 varied from 0.6 to 26%, with an annual average of 10%. The hourly ratio of
327 BC to PM$_{2.5}$ varied from 0.1 to 99%, with an annual mean of 12%. Compared
328 to a previous study conducted in the Yangtze River Delta, the BC/PM$_{2.5}$ ratio
329 in Nanjing was much higher than Shanghai (5.6%) (Wei et al., 2020),
330 implying a greater importance of primary emissions in Nanjing.

设置了格式: 字体: 倾斜

设置了格式: 下标
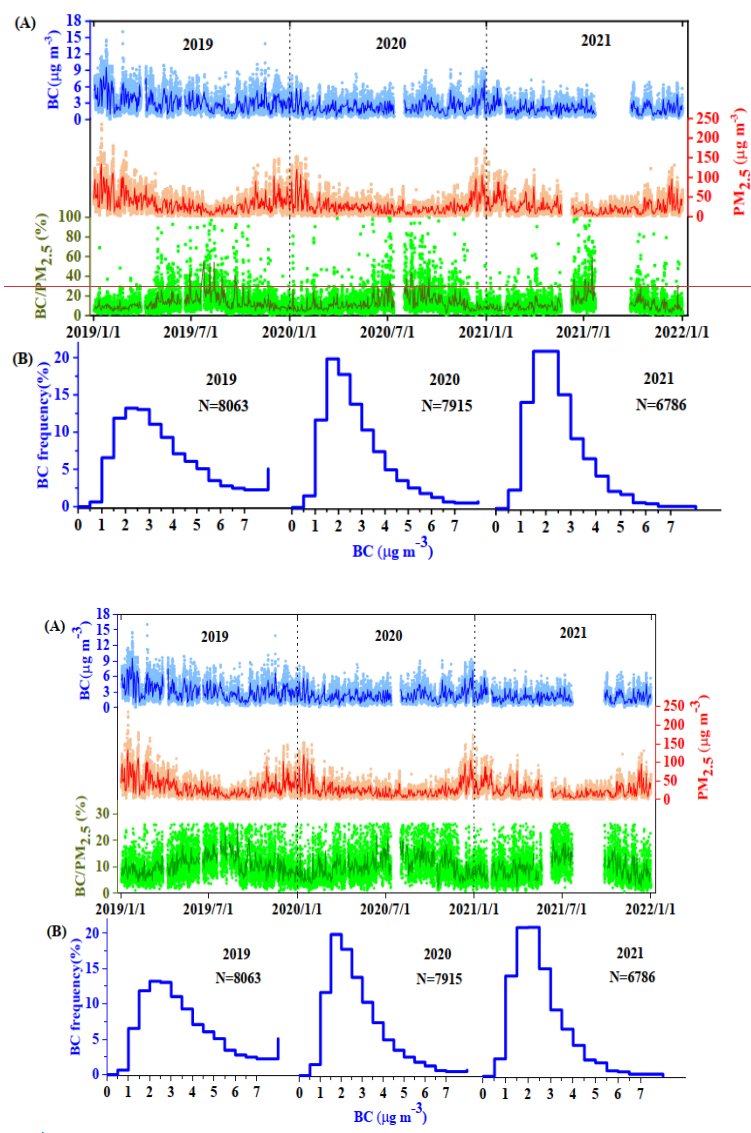
Figure 1 (A) Hourly (dots) and daily (line) concentration of BC, PM$_{2.5}$ and BC/PM$_{2.5}$ and (b) frequency

of BC for each year during 2019, 2020 and 2021. N represents number of hourly BC concentration for

one year

Table 2 listed long-time (equal or more than one year) BC mass concentrations monitored by optical method in Nanjing and other sampling sites around all over the world from previous studies. Nanjing's three-year

average BC level was the lowest among previous studies performed in Nanjing, indicating that primary emissions in Nanjing are decreasing year by year. While BC levels in other southern Chinese cities like Shanghai and Wuhan were at least 12.0% lower than those in Nanjing, they were at least 13.9% higher in northern Chinese cities like Beijing and Baoji. Additionally, BC concentrations in Nanjing were five times higher than in the baseline station Mt. Waliguan.

Table 2 Comparison of BC mass concentration in Nanjing with other sites

Location	Site type	Instrument	Study period (yyyy.mm)	BC ($\mu g\ m^{-3}$)	Reference
Nanjing, China	urban	AE33	2019.01-2021.12	2.52 ± 1.62	Present study
Nanjing, China	suburban	AE31	2012.01-2012.12	4.2 ± 2.6	(Zhuang et al., 2014)
Nanjing, China	urban	MAAP*	2017.12-2018.11	2.8 ± 2.0	(Zhang et al., 2020)
Mt. Waliguan, China	baseline	AE31	2008.01-2017.12	0.45 ± 0.37	(Dai et al., 2021)
Beijing, China	urban	AE31	2016.01-2016.12	3.4 ± 3.0	(Li et al., 2022)
Baoji, China	urban	AE31	2015.01-2015.12	2.9 ± 1.7	(Zhou et al., 2018)
Xianghe, China	rural	AE31	2013.04-2015.03	5.4 ± 4.4	(Ran et al., 2016)
Shanghai, China	urban	AE33	2017.01-2017.12	2.2 ± 1.3	(Wei et al., 2020)
Wuhan, China	urban	AE33	2013.06-2018.12	1.4 ± 1.2	(Zheng et al., 2020)
Panchgaon, India	suburban	AE42	2015.04-2016.03	7.2 ± 0.3	(Dumka et al., 2019)

格式化表格

351

Table 2 Comparison of BC mass concentration in Nanjing with other sites

Location	Site type	Instrument	Study period (yyyy.mm)	BC (µg m^{-3})	Reference
Nanjing, China	urban	AE33	2019.01-2021.12	2.52 ± 1.62	Present study
Nanjing, China	suburban	AE31	2012.01-2012.12	4.2 ± 2.6	(Zhuang et al., 2014)
Nanjing, China	urban	MAAP*	2017.12-2018.11	2.8 ± 2.0	(Zhang et al., 2020)
Mt. Waliguan, China	baseline	AE31	2008.01-2017.12	0.45 ± 0.37	(Dai et al., 2021)
Beijing, China	urban	AE31	2016.01-2016.12	3.4 ± 3.0	(Li et al., 2022)
Benxi, China	urban	AE31	2017.01-2017.12	2.9 ± 2.3	(Ding et al., 2024)
Baoji, China	urban	AE31	2015.01-2015.12	2.9 ± 1.7	(Zhou et al., 2018)
Xianghe, China	rural	AE31	2013.04-2015.03	5.4 ± 4.4	(Ran et al., 2016)
Shanghai, China	urban	AE33	2017.01-2017.12	2.2 ± 1.3	(Wei et al., 2020)
Wuhan, China	urban	AE33	2013.06-2018.12	1.4 ± 1.2	(Zheng et al., 2020)
Nanning, China	urban	AE31	2017.01-2017.12	1.0 ± 0.5	(Ding et al., 2023)
Panchgaon, India	suburban	AE42	2015.04-2016.03	7.2 ± 0.3	(Dumka et al., 2019)

352 *MAAP: Multi-angle absorption photometer

353 **3.2 Temporal variation of BC mass concentrations in Nanjing**

354 **3.2.1 Interannual, seasonal, and monthly variations**

355 The annual, seasonal, and monthly variations in BC mass concentrations
356 are illustrated in Figure 2. The annual average BC mass concentration in 2019
357 (3.2 ± 2.0 µg m^{-3}) was higher than in 2020 (2.3 ± 1.4 µg m^{-3}) and 2021 (2.0 ±
358 1.1 µg m^{-3}). A significant reduction of 28.1% in BC mass concentration was
359 observed from 2019 to 2020, much higher than the reduction (13.0%)
360 observed during 2020-2021. ~~Similarly~~ Consistent with BC, PM$_{2.5}$
361 concentrations reduced more sharply during 2019-2020 (24.1%) than in 2020-
362 2021 (6.2%). To prevent the spread of COVID-19, a series of lockdown
363 measures were imposed in China in late January 2020, resulting in a

14

364 remarkable decrease in concentrations of air pollutants (Bauwens et al., 2020;
365 Li et al., 2020; Wang et al., 2020).

366 Seasonally, the highest averaged BC level over three years occurred in
367 winter (2.9 ± 2.0 μg m^{-3}), with no obvious variation identified in spring (2.5
368 ± 1.5 μg m^{-3}), summer (2.4 ± 1.4 μg m^{-3}) or autumn (2.3 ± 1.5 μg m^{-3}),
369 suggesting a generally locally dominated source of BC emissions. The results
370 of bivariate polar plots showed the highest BC levels in low wind speed (WS
371 < 4 m s^{-1}) in all seasons (Figure ~~S2~~S4), further indicating that local sources
372 are the predominant contributors to atmospheric BC in Nanjing. High BC
373 mass concentrations in winter are mainly caused by enhanced emissions
374 during ~~due to~~ cold weather and deteriorating meteorological dispersion
375 conditions under~~resulting from~~ low temperatures. A similar seasonal pattern
376 was also found in previous studies conducted in other Yangtze River Delta
377 cities like Shanghai and Hefei (Chang et al., 2017; Zhang et al., 2015).
378 Seasonal average concentrations of BC varied from 1.83 (autumn of 2021) to
379 3.40 μg m^{-3} (spring of 2019) across different years. In 2019, BC concentration
380 in spring (3.4 ± 1.9 μg m^{-3}) was higher than in winter (2.6 ± 1.5 μg m^{-3}), likely
381 due to decreased human activities during the lockdown period. In contrast to
382 the spring of 2019, higher levels of BC were found in winter during 2020 and
383 2021.

384 The monthly mean concentrations of BC showed relatively large
385 variation, ranging from 1.6 (November of 2021) to 5.1 μg m^{-3}(January of
386 2019). The highest monthly average BC levels were found in January ($3.5 \pm$
387 2.3 μg m^{-3}), followed by December (2.9 ± 1.7 μg m^{-3}). The monthly variation
388 pattern of BC is consistent with previous studies in Nanjing, which reported
389 the highest BC levels in January and December (Zhang et al., 2020; Xiao et
390 al., 2020). Additionally, the BC concentration in January was 37% higher than
391 in August (2.2 ± 1.1 μg m^{-3}), attributed to relatively lower emission strength
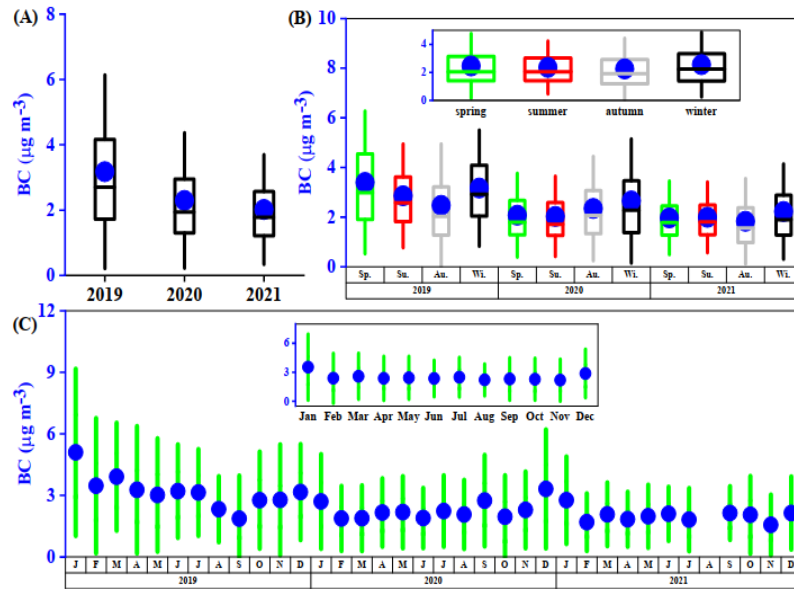392 and larger precipitation in summer in Nanjing.

393

Figure 2 (A) Interannual, (B) seasonal, and (C) monthly variations of BC. The relatively small figures
in (B) and (C) are overall average seasonal and monthly values. The blue dots represent average BC
values. The rectangles in (A) and (B) represent the 25% and 75% quantiles. The vertical lines in (A),
(B), and (C) represent 10% and 90% quantiles.

3.2.2 Diurnal variation of BC

The diurnal variations of BC mass concentrations for each year are
plotted in Figure. 3(a). The diurnal cycles of BC, like those in previous studies
conducted in Nanjing (Xiao et al., 2020; Zhang et al., 2020; Zhuang et al.,
2014), exhibited bimodal distributions in whole study period selected three
years. BC mass concentrations remained relatively flat at midnight and then
increased from 3:00 (local time, LT) to 7:00 LT. After reaching the highest
values at 7:00 LT, BC levels decreased, reaching the lowest values at 16:00
LT, then increased again, and maintaineding higher values in the evening. The
bimodal diurnal patterns of BC were attributed to the intensity of emissions
and variations in meteorological conditions (Cao et al., 2009). The morning
peak of BC was mainly caused by vehicle emissions during the traffic rush
hour, as indicated by the similar diurnal cycles of CO and NO_2 also showing
similar diurnal cycles to BC (Figure S3S5). After the morning peak, the
boundary layer height developed and WS increased, increasing atmospheric

16

dilution capability and lowering the BC levels. After 14:00 LT, due to a decrease in boundary layer height and WS, BC was gathered on the surface layer, resulting in higher BC loading from evening to midnight. The peak BC concentration in 2019 was 29%, 38% higher than in 2020 and 2021 respectively, indicating~~es~~ air quality in Nanjing is getting better due to the strict implementation of air pollution control plans. Additionally, the impact of COVID-19 lockdown measures during selected years ~~have~~ has also contributed to the reduction in BC concentrations.

To further explore the impacts of human activities on ambient BC concentrations, the diurnal variation in BC was separately investigated for weekdays and weekends. As shown in Figure 3(b), the diurnal patterns of BC on both weekdays and weekends exhibited bimodal distributions, with similar peak times at morning vehicle rush hours (7:00 LT), suggesting that local emission sources of BC in northern Nanjing do not differ significantly between weekdays and weekends.
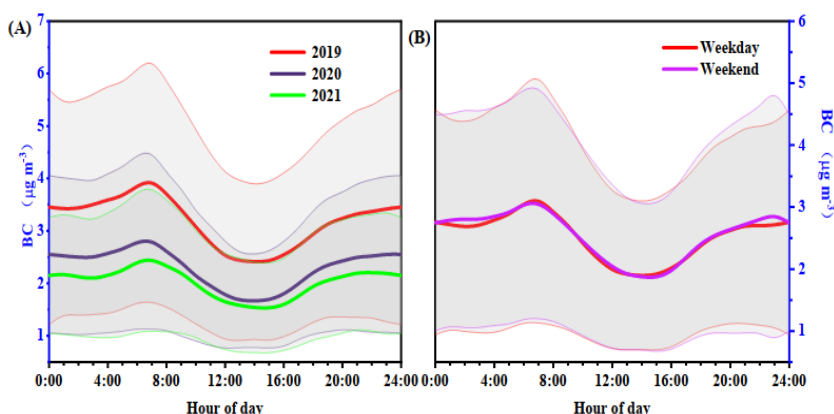
Figure 3 Diurnal variation of BC (A) for each year during 2019-2020 and (B) during weekdays and weekends. Shaded areas represent the standard deviation at each time of day.

3.3 Source apportionment of BC

3.3.1 Source apportionment of BC by Aethalometer model

The AAE values, calculated by power-law fit between light absorbance and seven wavelengths, followed a lognormal distribution in ~~selected~~ three years, with an hourly variation ranging from 0.71 to 2.59 (Figure ~~S4~~S6). The three-year average AAE value was 1.25 ± 0.14, with the highest value of 1.28

± 0.13 in 2021, ~~slightly~~ which was 4.0% and 4.3% higher than those ~~by 4.0% and 4.3%~~ in 2019 and 2020, respectively, indicating similar BC emission sources during the sampling period. Seasonally, the lowest AAE value of 1.13 ± 0.14 was found in summer, while the highest AAE value of 1.32 ± 0.11 appeared in winter. The monthly variation of AAE showed a valley in the summer months (particularly in July) and high values in winter (December), suggesting that Nanjing was predominantly influenced by traffic-related liquid fuel burning in summer, and coal-related combustion in winter.

To quantify the relative contribution of liquid and solid fuel combustion to BC concentration, the Aethalometer model, as mentioned in section 2.2, was applied. The Aethalometer model was initially used for BC source apportion ~~BC~~ in Europe, where fossil fuel and biomass burning emissions were two major sources. However, China's energy structure differs from Europe's, with coal combustion still playing a significant role. Liu et al. (2018) summarized AAE values from different coal burning sources in China, finding that AAE values of coal burning were close to those of biomass combustion. Thus, AAE values of 1.0 for liquid fuel (AAE_{liquid}) and 2.0 for solid fuel (AAE_{solid}) were selected for this work. The same AAE pairs were also used for source apportionment of BC in a previous study carried out in Nanjing (Lin et al., 2021). Figure 4 shows the time series of absolute BC concentrations derived from liquid and solid fuel combustion, along with a depiction of their relative contributions to BC in different seasons for each year. The three-year average concentration of BC_{liquid} was $2.0 ± 0.5\mu g\ m^{-3}$, approximately four times that of BC_{solid}. Liquid fuel combustion is the dominant source of BC in Nanjing, with 79% of BC generated from the consumption of liquid fuel. Interannually, the contributions of liquid fuel ranged from 76% to 81%, ~~results that are~~ which is comparable to other cities in China such as Wuhan (81%) and Shanghai (88-94%) (Zheng et al., 2020; Wei et al., 2020). The contribution of liquid fuel burning to BC was highest in summer (85%), in contrast to the lowest value ~~appear~~osbserved in winter (72%), much higher than that of Beijing (35.7%) (Li et al., 2022). Beijing is heavily affected by heating activities in winter, such as power plants and residential heating using coal and biomass, resulting in higher solid fuel emissions. The seasonal average contribution of BB varied by 5%~~,~~ (~~-~~from 19% to 24%), influenced by coal-fired emissions from surrounding factories and

long-range transport of domestic cooking emissions in rural areas in the Yangtze River Delta region (Wei et al., 2020).
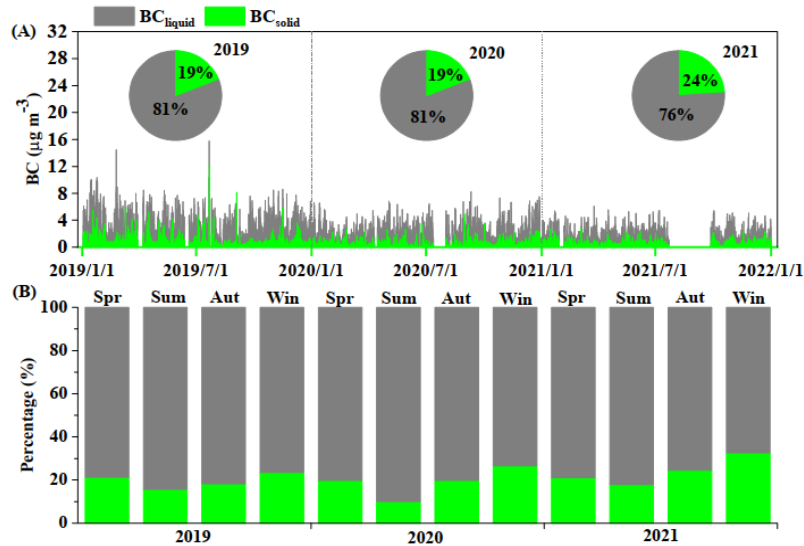

Figure 4 (A) Hourly variation of BC_{liquid} and BC_{solid}, and (B) their relative contribution to BC. The pie charts in (A) are annual average relative contribution of BC_{liquid} and BC_{solid} to BC.

It is important to highlight that the results of the Aethalometer model are highly dependent on the determination of AAE values, with AAE_{liquid} ranging frombetween 0.8 to 1.1, and AAE_{solid} values ranging frombetween 1.8 to 2.2, as widely used in this model (Helin et al., 2018; Dumka et al., 2019; Fuller et al., 2014). To estimate the uncertainty of the Aethalometer model, we calculated source apportionment results using different AAE pairs, the results are showedshown in Table S1. And aAn uncertainty estimation of 11.0% for the BC_{liquid} was found Aethalometer model results in this work. Although there are uncertainties in source apportionment results, our results indicate that liquid fuel combustion is the main source of BC in Nanjing during the study period.

3.3.2 Source diagnostic tracers

The ratios of $BC/PM_{2.5}$ and BC/CO (carbon monoxide, CO) have been utilized to estimate emission sources in previous studies since they can vary when emitted from different sources (Chow et al., 2011; Zhang et al., 2009). The proportion of BC in $PM_{2.5}$ is higher in traffic sources than that from other

19

sources (such as residential coal combustion and forest fire). As listed in Table S2, higher BC/PM$_{2.5}$ ratios were found in heavy-duty diesel (33-74%) and light-duty diesel (62-64%), followed by those from agricultural burning (6-13%) and forest fire (3%) (Table S2) (Chow et al., 2011). The highest ratio of BC/PM$_{2.5}$ appeared in autumn time (20%) while the lowest was observed in winter (8%), suggesting an increase ind biomass and coal burning during in winter. Previous studies reported that the ratio of BC/CO was lower in traffic emissions, as compared to the ratios from industry, power plant, residential and traffic emissions were 0.72%, 1.77%, 3.71%, and 0.52%, respectively (Table S2) (Zhang et al., 2009). The average ratios of BC/CO in spring, summer, autumn, and winter were 0.39%, 0.49%, 0.49%, and 0.31%, respectively, further suggesting that the traffic source was dominant in Nanjing (Table 3).

To further support the source apportionment results of BC, a correlation analysis was conducted between BC and trace gases such as SO$_2$, and NO$_2$, mainly derived from coal combustion, and vehicles emissions respectively. As listed in Table 3, the correlations of BC with NO$_2$ (0.54-0.67) were higher than the correlations of BC with SO$_2$ (0.16-0.59), further indicating the dominance of traffic emission in Nanjing.

Table 3 Mass ratios and correlations between BC and other pollutants

		Spring	Summer	Autumn	Winter	Annual
Mass ratios (%)	BC/PM$_{2.5}$	12.93	10.63	19.64	7.92	12.78
	BC/CO	0.39	0.49	0.49	0.31	0.42
Correlation	BC-SO$_2$	0.49	0.16	0.32	0.59	0.38
	BC-NO$_2$	0.66	0.61	0.54	0.67	0.60

3.4 Long-term trend of BC

3.4.1 Black carbon simulation results

After training the RF models with optimal hyperparameters, the models for BC at 880 nm and 370 nm were evaluated on test sets to assess predictive performance. The density scatter plot as displayed in Figure 5 showed shows the relationship between the test set and the RF model predictions. that the RF model accurately reproduced hourly BC concentrations at both wavelengths. The RF model explained over 90% of the variation in BC concentrations, achieving an R² of 0.92 between the

monitored and predicted results at both 370 and 880 nm. At the 370 nm wavelength, the RMSE was 0.57 μg m⁻³, which was 22.8% higher than the RMSE at 880 nm, likely due to the higher observed BC levels at this wavelength. The results showed that the RF model explained over 90% of the variation in BC concentrations, with R^2 values of 0.90 and 0.91 between the monitored and predicted results at both 370 and 880 nm, respectively. The RF model's predictions for the test dataset were close to those for the training dataset, indicating consistent performance across both datasets and demonstrating its stability and reliability. In addition to evaluating the RF model using the test set, further validation was conducted using Tracking Air Pollution in China (TAP) (10 km × 10 km, http://tapdata.org.cn) data. The predicted BC values at 880 nm from the RF model showed good agreement with the TAP dataset, with an R^2 of 0.72 (Figure S5S7). Using the trained model and available predictors, hourly BC concentration at the sampling site can be accurately reconstructed for any given period, consistent with AE33.
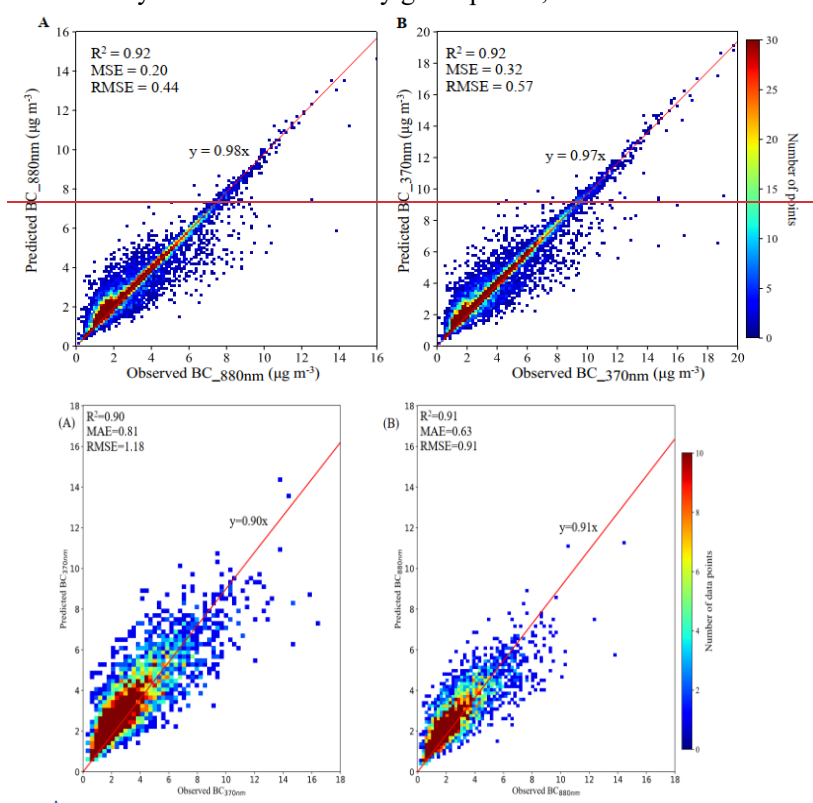
Figure 5 Density scatter plots of hourly observed and modeled BC at (a) 880 370 nm and (b) 370 880 nm from the test dataset

After training the RF models with input data, Shapley Additive exPlanations (SHAP) values were used to assess the importance of each predictors on model outcomes (Lundberg and Lee, 2017). Figure S6 S8 presentsed the ranked average SHAP values for each predictor for BC at the two wavelengths. NO_2, BLH and SO_2 were identified as having the greatest impact on model's prediction. As withSimilar to BC, NO_2 and SO_2 are primarily emitted from incomplete combustion processes involving fossil fuels (Lee et al., 2017; Yao et al., 2002). As a result, BC, NO_2 and SO_2 are often co-emitted by factories or traffic near the sampling site. BLH determines the diffusion capacity of the atmosphere; a lower BLH means stronger atmospheric stability, resulting in increased BC levels inon the surface air. Unlike BLH, the contribution of other meteorology predictors such as T, RH, WS and WD, were relatively low compared to pollutant gases. One possible reason for this is meteorological condition changes may not have an immediate effect on atmospheric BC levels; instead, there may be a certain lag in their effects.

3.4.2 Long-term temporal variation of BC

Meteorological data and air pollutants concentrations were used in the trained RF model to estimate BC concentrations at 370 and 880 nm from 2014 to 2021. The Aethalometer Model, using AAE of 1 and 2, was then applied to the simulated BC to explore the long-term temporal variation of source-specific BC. It is important to highlight that the results of the Aethalometer model are highly dependent on the determination of AAE values, with AAE_{liqiud} ranges between 0.8 to 1.1 , and AAE_{solid} ranges between 1.8 to 2.2, as widely used in this model (Helin et al., 2018; Dumka et al., 2019; Fuller et al., 2014; Jing et al., 2019). To assess the model's uncertainty, source apportionment was conducted using various AAE pairs (Figure S9). The results revealed that liquid fuel remained a dominant source of BC even when different AAE paired values were used, with the pattern of source apportionment results consistent across different AAE combinations. The AAE_{liqiud} = 1 and AAE_{solid} = 2 were used in this study, as the same combination of AAE values were utilized in Nanjing and other sites in China (Ding et al., 2024; Liu et al., 2018; Lin et al., 2021). Additionally, the

设置了格式: 下标

设置了格式: 下标
设置了格式: 下标

22

uncertainty of source apportionment was estimated based on the relative differences between results obtained with other AAE values and those set to 1 and 2. As a result, the uncertainty of the BC_{liquid} was estimated to be 10%. Between 2014 and 2021, average BC concentrations decreased by 35.7% from 3.12 ± 1.39 μg m^{-3} in 2014 to 2.04 ± 0.33 μg m^{-3} in 2021. The statistical significance of the reduction in BC and source-specific BC was assessed using the Mann-Kendall test on monthly median values, with results presented~~shown~~ in Figure 6. A significant decreasing trend ($p<0.01$) in BC concentrations was observed, with a slope of -0.13 μg m^{-3}yr^{-1}. Similar reductions have also been reported across various regions in China since 2013 (He et al., 2023; Sun et al., 2022a; Chow et al., 2022; Dai et al., 2023). ~~Significantly~~Significant decreases were also observed in BC_{liquid} ($p<0.01$) and BC_{solid} ($p<0.05$) concentrations. From 2014 to 2021, BC_{liquid}~~,~~ decreased by 38.4% (from 2.55 ± 1.14 μg m^{-3} to 1.57 ± 0.89 μg m^{-3} in 2021) at an absolute rate of -0.10 μg m^{-3}yr^{-1}, while BC_{solid} decreased by 20.3% (from 0.59 ± 0.52 μg m^{-3} to 0.47 ± 0.33 μg m^{-3}) at a rate of -0.03 μg m^{-3}yr^{-1}. The contributions of different sources to the overall BC reduction were estimated by comparing the absolute decrease slopes of BC_{liquid} and BC_{solid} to the overall BC decrease slope. It was found that 77~~-~~% of total BC reduction was due to the decreased liquid fuel combustion, highlighting the significant role of BC_{liquid} in reducing BC concentrations from 2014 to 2021. Pollutants commonly co-emitted with BC, such as NO_2, CO and SO_2, exhibited significant declining trends ($p < 0.05$) during the study period (Figure S10). In contrast, the $BC/PM_{2.5}$ ratio showed a significant increasing trend ($p < 0.01$), suggesting that while emission reduction policies have been effective in decreasing precursors of secondary aerosol (SO_4^{2-}, NO_3^-, NH_4^+), stricter regulations on BC emissions may also be necessary. The variation in the BC/CO ratio was not significant, with the mean value remaining stable at approximately 0.38% throughout the period.

Throughout the study period, BC concentrations exhibited two distinct declining ~~decrease~~ trends, which aligned~~ed~~ with the implementation of the Air Pollution and Control Action Plan (2013-2017, P1) and the Three-Year Action Plan (starting in 2018, P2) by the Chinese government. To compare the decreasing trends of BC in the two periods, the absolute trends were normalized by the average values for each period. The change rates of BC and

other air pollutants are shown in Table 4. During P1, the relative slopes of BC and BC_{liquid} were -4.18 % yr^{-1} ($p < 0.1$) and -4.26 % yr^{-1} ($p < 0.05$), respectively, with BC_{liquid} accounted for 83% of the total decrease in atmospheric BC concentrations. Since the decrease in BC_{solid} is ~~not~~ insignificant, the actual contribution of BC_{liquid} may be higher than estimated. Compared to P1, the decline in BC, BC_{liquid} and BC_{solid} concentration during P2 was much steeper, reaching -~~10.9~~11.2 % yr^{-1} ($p < 0.01$), -9.~~7~~10.3 % yr^{-1} ($p < 0.01$) and -11.~~1~~6 % yr^{-1} ($p < 0.1$), respectively. In the S2 period, reductions in both BC_{liquid} and BC_{solid} contributed to the overall decrease in BC concentration, with BC_{liquid} still being the dominant factor, accounting for ~~71~~72% of the total reduction. SO2 and NO2, which shared the same sources as BC, also decreased more rapidly in S2 (-~~31~~33.6~~2~~ % yr^{-1} and -8.~~5~~7 % yr^{-1}) compared to S1 (-~~9.3~~10.1 % yr^{-1} and -~~0.7~~1.26 % yr^{-1}), suggesting that air pollutants have been decreasing much faster after 2018 than before.
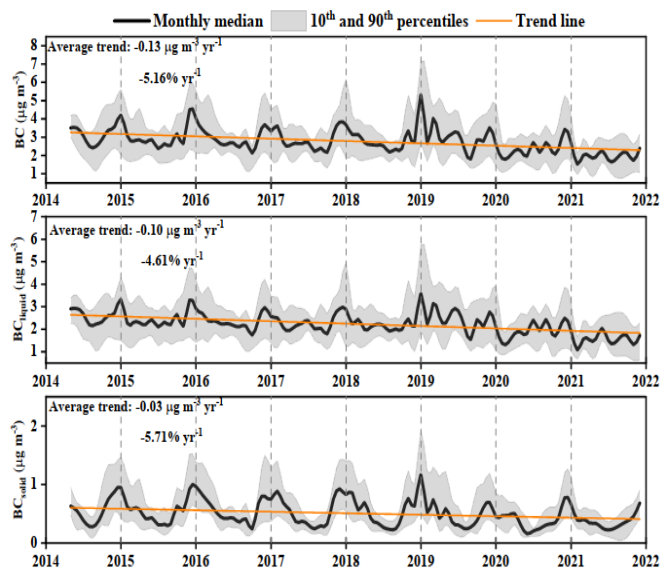

Figure 6 Trends in BC, BC_{liquid} and BC_{solid} at sampling site. The solid black line represents the monthly medians, the dash black lines represent the 10th and 90th monthly percentiles, and the orange line is the fitted long-term trend.

设置了格式: 字体: (默认) +西文正文 (等线)

带格式的: 正文, 行距: 单倍行距

631

Table 4 The change rates of BC and other air pollutants during different periods

Study period	air pollutants	absolute slope[a]	relative slope[b]	p
Air Pollution Prevention and Control Action Plan	BC	-0.12	-4.18%	0.08
	BC_{liquid}	-0.10	-4.26%	0.02
	BC_{solid}	-0.02	-3.48%	0.6
	$PM_{2.5}$	-12.00	-26.29%	0.0001
	NO_2	-0.46	-1.26%	0.74
	SO_2	-1.69	-10.08%	0.06
	CO	0.02	1.76%	0.62
After 2018	BC	-0.29	-11.22%	0.0002
	BC_{liquid}	-0.21	-10.26%	0.0001
	BC_{solid}	-0.05	-11.55%	0.06
	$PM_{2.5}$	-4.62	-17.20%	0.0009
	NO_2	-2.91	-8.73%	0.02
	SO_2	-2.32	-33.23%	0.0001
	CO	0.00	0.00%	0.66

632 [a]: $\mu g\ m^{-3}\ yr^{-1}$

633 [b]: $\%\ yr^{-1}$

634 The seasonal trends in BC and its different sources were further
635 investigated in Nanjing. As shown in Figure 7, significant reductions in BC
636 concentrations were observed across all seasons. The decreasing slopes of BC
637 in spring (-7.2 % yr^{-1}, $p < 0.01$) and winter (-10.6 % yr^{-1}, $p < 0.01$)
638 were steeper than those in summer (-5.07 % yr^{-1}, $p < 0.05$) and autumn (-

25

43.9 % yr^{-1}, $p < 0.05$1). The reduction rate of PM$_{2.5}$ in spring (-1815.9 % yr-1, $p < 0.05$01), summer (-2225.54%, $p < 0.05$01) and autumn (-15.920.0 % yr-1, $p < 0.01$) was 3 to 6 times that of BC (Table S3). In winter, the reduction rate (-914.8-2 % yr-1, p < 0.01) is closer to that of BC, suggesting that the reduction of primary pollutants in Nanjing during winter might be more effective than incompared to other seasons. The seasonal variation of BC$_{liquid}$ showed distinct trends across different seasons. Significant reductions were observed in spring, summer, autumn and winter, with the absolute slope of -5.97.6 % yr-1 ($p < 0.01$), -4.13.8 % yr-1 ($p < 0.05$), and -5.16.5 % yr-1 ($p < 0.01$5) and -10.5 % yr-1 ($p < 0.01$), respectively. The reduction reate of BC$_{liquid}$ in summer was the lowest compared to other seasons, potentially attributable to increased traffic activity associated with the peak tourism season. BC$_{liquid}$ in summer was not statistically significant, which may be partly due to increased traffic activity during tourism peak season, leading to higher liquid fuel consumption. Moreover, the reduction rate of PM$_{2.5}$ was faster in summer compared to BC, indicating that secondary aerosol reductions were more pronounced during this season. BC$_{solid}$ showed a similar decreasing slope in summer spring (-6.18.7 % yr-1, $p < 0.05$1), and winter (-8.56.2 % yr-1, $p < 0.01$5), while summerautumn appeared relatively higherslower reduction (-12.24.2 % yr-1, $p < 0.01$). The more pronounced decline of BC$_{solid}$ during the summer can be attributed to the seasonal variation in significant BC$_{solid}$ emission sources in Nanjing, such as biomass burning activities, which are minimal during this period. Similar to BC$_{solid}$, SO$_2$ exhibited a steeper change rate in winter (-24.4 % yr-1, p < 0.01) and a slower change rate in autumn (-16.2 % yr-1, p < 0.01) (Table S3). The reduction of BC$_{solid}$ in autumn spring was not insignificant, which may be influenced by long-range transport of biomass burning, as well as increased agricultural activities during this season. It is worth noting that BC$_{liquid}$ contributed 76%92% to overallthe overall BC reduction in autumn. spring and BC$_{solid}$ contributed 25% to overall BC reduction in summer. However, since the decreasing trend of BC$_{solid}$ in autumnspring and BC$_{liquid}$ in summer were was not statistically significant, these contributions may have been underestimated.
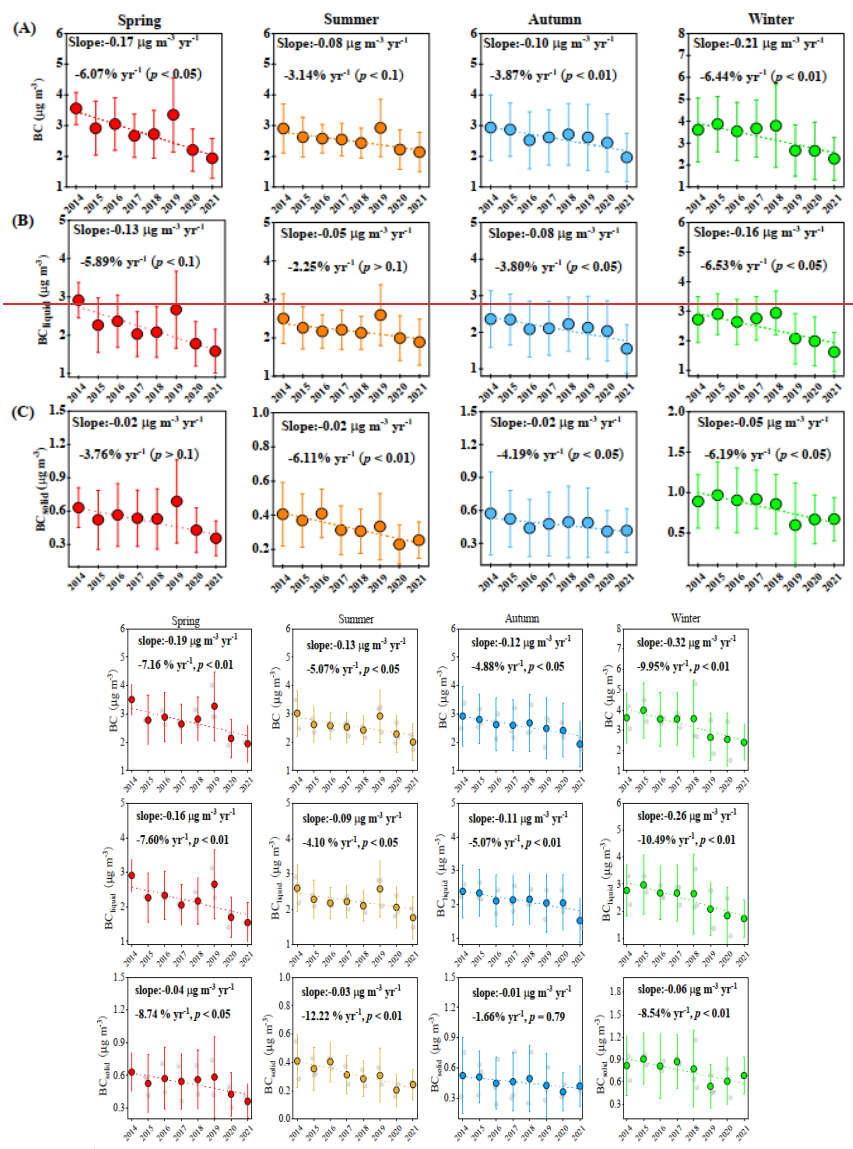
671

672

Figure 7 Seasonal variation of (A) BC, (B) BC$_{liquid}$ and (C) BC$_{solid}$ in spring, summer, autumn and winter. The circle in different colors represents the average concentration of BC, BC$_{liquid}$ and BC$_{solid}$. The vertical lines represent the standard deviations of BC, BC$_{liquid}$ and BC$_{solid}$. The grey circles in each panel represent the monthly average values.

3.4.3 The impact of Emission and Meteorology

In addition to changes in emissions, meteorological conditions can also

affect the long-term trends of pollutants by influencing their long-range transport and processes of dry and wet deposition. To explore these impacts on the long-term trends of BC, the KZ filter was applied to distinguish between emission-related (E_{LT}^{emi}) and meteorology-related (E_{LT}^{met}) trends. The daily averaged log-transformed original time series along with decoupled short-term, baseline and seasonal of BC were described in Figure ~~S7~~S11. The short-term component of BC displayed notable fluctuations, while the seasonal component showed a clear cycle with higher levels in winter and lower levels in summer. The largest variances for BC (69%), BC_{liquid} (73%) and BC_{solid} (52%) were found in the short-term component, reflecting the essential role of synoptic weather on the daily variations of primary aerosol content in Nanjing (Table S4). BC_{solid} exhibits seasonal dependence with relatively higher seasonal component (40%) than BC (16%) and BC_{liquid} (12%). The sum of variances explained by the short-term, seasonal and long-term component for BC, BC_{liquid} and BC_{solid} ~~were~~ was 93%, 92% and 92%, respectively. A total variance close to 100% ~~indicating~~ indicates that these three components are largely independent of each other, ~~–~~suggesting that most of the meteorological influence ~~have~~ has been effectively accounted and removed (Chen et al., 2019; Sun et al., 2022b; Zheng et al., 2020). To separate emission-related (E_{LT}^{emi}) and meteorology-related components (E_{LT}^{met}) from the long-term component (E_{LT}), multiple linear regression was conducted using the baseline component of meteorological parameters and BC. The model incorporating these meteorological parameters accurately reproduced the baseline of BC_{solid} ($R^2 = 0.84$, $p < 0.001$). In contrast, it was less effective in explaining the baseline for BC ($R^2 = 0.59$, $p < 0.001$) and BC_{liquid} ($R^2 = 0.51$, $p < 0.001$), suggesting that local emission changes across different seasons play an important role in impacting BC and BC_{liquid} in Nanjing.

Fihure S11 exhibited the long-term variation of E_{LT}^{emi} and E_{LT}^{met} for BC, BC_{liquid} and BC_{solid}, and the corresponding linear trends were summarized in Table 5. ~~The linear trends of E_{LT}, E_{LT}^{emi} and E_{LT}^{met} for BC, BC_{liquid} and BC_{solid} are summarized in Table 5.~~ It is important to note that the linear trend slope of E_{LT} represents relative change rate (% yr^{-1}) of the baseline concentration, since original time series of BC ~~were~~ was log-transformed before applying the KZ filter. To con~~ve~~ert the fractional change rate into an absolute change

28

rate ($\mu g\ m^{-3}\ yr^{-1}$), it is multiplied by the average baseline concentration (not log-transformed). The E_{LT} of BC and its distinct source exhibited significant ($p < 0.01$) declining trends, with slopes of -0.1, -0.08 and -0.02 ug m^{-3} yr^{-1} for BC, BC_{liquid} and BC_{solid}, respectively. BC_{liquid} was the dominant contributor to BC reduction, accounting for 80% of the overall decrease, suggesting that when the influence of seasonal and synoptic variations is excluded, its contribution to BC temporal variations becomes more evident. The emission-related components of BC, BC_{liquid} and BC_{solid} exhibited similar long-term trends (Figure S12). From 2014 to 2016, the emission-related trends remained relatively stable, reaching a lower level by the end of 2017. Subsequently, the emission-related components of BC, BC_{liquid} and BC_{solid} increased, peaking in 2019, followed by a sharp decline until mid-2020, and then rebounding to another peak at the end of 2021, which may be related to the recovery of production activities following the pandemic. In contrast, meteorology-related trends of BC and BC_{liquid} showed a sharp decrease after 2020, while BC_{solid} exhibited a downward trend between 2014 and 2021, with meteorology-related trends of BC_{solid} followed a fluctuating downward pattern. In addition, the relative contributions of E_{LT}^{emi} and E_{LT}^{met} to BC reduction were quantified by calculating the ratio of their absolute slopes to that of E_{LT} (Zheng et al., 2023). Both meteorologymeteorological conditions and emission reductions played crucial roles in reducing BC and its specific sources. Emission reductions were found to be the major contributor to the decline in long-term trends of BC, BC_{liquid} and BC_{solid}, with contributions of 70%, 63% and 86%, respectively. While emissions reductions dominated the decrease in BC concentrations throughout the study period, their relative influence compared to meteorological conditions varied between the P1 (before 2018) and P2 (after 2018) phases. As shown in Figure 8, emission reductions played a more prominent role, contributing 78%, 62% and 86% to the reductions in BC, BC_{liquid} and BC_{solid}, respectively. However, during P2, meteorological conditions played a leading role in reducing BC and BC_{liquid}, contributing 66% and 70%, respectively. Moreover, meteorology condition had a notable impact on BC_{solid} in P2, with its contribution increasing from 14% in P1 to 31%. This suggests that the rapid reduction of BC in P2 was largely due to favorable meteorological conditions, which played a crucial role in facilitating its decline. It is worth noting that the impact of

meteorological conditions on BC_{liquid} and BC_{solid} differs significantly, especially in P2. While meteorology contributed 70% to the reduction in BC_{liquid}, its impact on BC_{solid} was only 31%. This difference is because BC_{liquid}, mainly from vehicle exhaust, remains stable year-round, whereas BC_{solid}, from activities like biomass burning and coal combustion, varies seasonally. The results of significance analysis further confirmed that there was no significant difference in BC_{liquid} and BC_{solid} while significant ($p < 0.05$) differences were observed in autumn and winter, when BC_{solid} emissions are more pronounced due to increased biomass burning and coal combustion activities (Figure S13). This seasonal variability in emission sources explains the differing impacts of meteorology on BC_{liquid} and BC_{solid}.

Table 5 Linear trends of long-term component of BC and its sources including BC_{liquid} and BC_{solid}

Components	BC			BC_{liquid}			BC_{solid}		
	absolute[a]	relative[b]	p	absolute[a]	relative[b]	p	absolute[a]	relative[b]	p
E_{LT}	-0.10	-3.76	0.01	-0.08	-3.54	0.01	-0.014	-4.91	0.01
E_{LT}^{EMI}	-0.07	-2.63	0.01	-0.05	-2.20	0.01	-0.012	-3.62	0.01
E_{LT}^{MET}	-0.03	-1.13	0.01	-0.03	-1.32	0.01	-0.002	-1.27	0.01

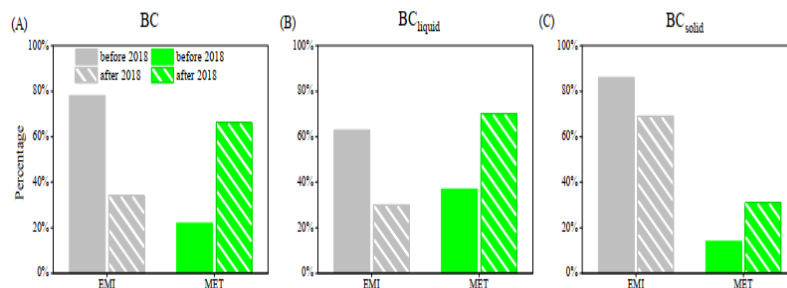[a]: $\mu g\ m^{-3}\ yr^{-1}$

[b]: % yr-1

Figure 8 Contributions of Emission Reduction Policies and Meteorological Conditions to the Decrease in BC Concentrations Before and After 2018. The (A), (B) and (C) panels represent BC, BC_{liquid} and BC_{solid}.

4. Conclusion

In this work, BC mass concentrations were continuously monitored in Nanjing, China, from 2019 to 2021. Combining observations with random forest algorithmalgorithms, the BC concentrations from 2014-2021 were reconstructed to explore the long-term trends of BC and its sources during

two distinct emission reduction periods. The results showed that BC concentrations were analyzed to reveal its characteristics and sources. The annual average BC mass concentration during the study period was $2.5 \pm 1.6\mu g\ m^{-3}$. Relatively higher BC mass concentrations were found in winter, while no clear variation was observed during other seasons, implying a locally dominant BC source. Diurnal variations showed a bimodal pattern with lower concentrations in daytime and higher values ~~in~~at night, primarily influenced by traffic rush hours and boundary layer heights. Liquid fuel combustion contributed more than 75% to BC in all years, with the highest contribution appearing in summer (85%) and the lowest in winter (72%).

The RF models explained over 90% variation and accurately captured seasonal cycle well of BC at both wavelength ~~880 nm~~, demonstrating the strong predictive capability of the trained models. The long-term trend of BC, BC_{liquid} and BC_{solid} all exhibited significant ($p < 0.05$) declines, with BC_{liquid} contributing the most to the overall BC reduction, accounting for 77% of the total decrease over entire period. Notably, BC levels decreased most rapidly during winter, while the reduction in summer was much slower. The trend in BC reduction varied between two distinct phases, in P2 (after 2018), BC levels declined much steeper compared to that in P1 (2014-2017), indicating that policies aimed at replacing coal to cleaner energy have been particularly effective in reducing primary pollutants. Over the entire period, emission reduction was the primary driver of BC reduction, contributing to BC, BC_{liquid} and BC_{solid} reduction, with contribution of 70%, 63%, and 86%, ~~respevtively,~~ respectively, ~~—~~while meteorological conditions accounted for 30%, 37% and 24%. Although emission reduction dominated BC reduction over the entire period, the contributions of emission reduction and meteorological conditions to BC reduction differed between the two phases. In P1, emission reduction played a dominant role, while in P2, meteorological conditions became the primary driver of BC reduction. Our results highlight that to further reduce atmospheric BC, targeted policies should be implemented to restrict liquid fuel combustion, especially during the summer. Additionally, the impact of meteorological factors on BC concentrations should not be overlooked during emission reduction efforts.

Data Availability

The hourly meteorological reanalysis data ERA5 are available in the ECMWF

at https://cds.climate.copernicus.eu/cdsapp#!/dataset/reanalysis-era5-single-levels?tab=form. Hourly averaged concentrations of $PM_{2.5}$, CO, SO_2 and NO_2 were obtained from https://quotsoft.net/air/. All the observational and predicted data were openly accessible at the Open Science Framework https://osf.io/8n32t/.

Competing interests

The contact author has declared that none of the authors has any competing interests.

Author contributions

Yanlin Zhang designed the research. Fang Cao, Mingyuan Yu, and Chaman Gul took part in data analysis and revised and commented on the paper. Abudurexiati·Abulimiti wrote the paper. Yihang Hong ~~analysis~~analyses the data. All authors contributed to the discussion of this paper.

Acknowledgement

References

Bauwens, M., Compernolle, S., Stavrakou, T., Müller, J.-F., van Gent, J., Eskes, H., Levelt, P. F., van der A, R., Veefkind, J. P., Vlietinck, J., Yu, H., and Zehner, C.: Impact of Coronavirus Outbreak on NO2 Pollution Assessed Using TROPOMI and OMI Observations, Geophysical Research Letters, 47, e2020GL087978, https://doi.org/10.1029/2020GL087978, 2020.

Bond, T. C., Doherty, S. J., Fahey, D. W., Forster, P. M., Berntsen, T., DeAngelo, B. J., Flanner, M. G., Ghan, S., Kärcher, B., Koch, D., Kinne, S., Kondo, Y., Quinn, P. K., Sarofim, M. C., Schultz, M. G., Schulz, M., Venkataraman, C., Zhang, H., Zhang, S., Bellouin, N., Guttikunda, S. K., Hopke, P. K., Jacobson, M. Z., Kaiser, J. W., Klimont, Z., Lohmann, U., Schwarz, J. P., Shindell, D., Storelvmo, T., Warren, S. G., and Zender, C. S.: Bounding the role of black carbon in the climate system: A scientific assessment, Journal of Geophysical Research: Atmospheres, 118, 5380-5552, https://doi.org/10.1002/jgrd.50171, 2013.

Cao, J. J., Zhu, C. S., Chow, J. C., Watson, J. G., Han, Y. M., Wang, G. h., Shen, Z. x., and An, Z. S.: Black carbon relationships with emissions and meteorology in Xi'an, China, Atmospheric Research, 94, 194-202, https://doi.org/10.1016/j.atmosres.2009.05.009, 2009.

Chang, Y., Deng, C., Cao, F., Cao, C., Zou, Z., Liu, S., Lee, X., Li, J., Zhang, G., and Zhang, Y.: Assessment of carbonaceous aerosols in Shanghai, China – Part 1: long-term evolution, seasonal variations, and meteorological effects, Atmos. Chem. Phys., 17, 9945-9964, 10.5194/acp-17-9945-2017, 2017.

Chen, Z., Chen, D., Kwan, M. P., Chen, B., Gao, B., Zhuang, Y., Li, R., and Xu, B.: The control of anthropogenic emissions contributed to 80 % of the decrease in PM2.5 concentrations in Beijing from 2013 to 2017, Atmos. Chem. Phys., 19, 13519-13533, 10.5194/acp-19-13519-2019, 2019.

846 Cheng, J., Su, J., Cui, T., Li, X., Dong, X., Sun, F., Yang, Y., Tong, D., Zheng, Y., Li, Y., Li, J., Zhang, Q.,
847 and He, K.: Dominant role of emission reduction in PM2.5 air quality improvement in Beijing during
848 2013–2017: a model-based decomposition analysis, Atmos. Chem. Phys., 19, 6125-6146,
849 10.5194/acp-19-6125-2019, 2019.
850 Chow, J. C., Watson, J. G., Lowenthal, D. H., Antony Chen, L. W., and Motallebi, N.: PM2.5 source
851 profiles for black and organic carbon emission inventories, Atmospheric Environment, 45, 5407-
852 5414, https://doi.org/10.1016/j.atmosenv.2011.07.011, 2011.
853 Chow, W. S., Liao, K., Huang, X. H. H., Leung, K. F., Lau, A. K. H., and Yu, J. Z.: Measurement report:
854 The 10-year trend of PM2.5 major components and source tracers from 2008 to 2017 in an urban
855 site of Hong Kong, China, Atmos. Chem. Phys., 22, 11557-11577, 10.5194/acp-22-11557-2022,
856 2022.
857 Dai, M., Zhu, B., Fang, C., Zhou, S., Lu, W., Zhao, D., Ding, D., Pan, C., and Liao, H.: Long-Term
858 Variation and Source Apportionment of Black Carbon at Mt. Waliguan, China, Journal of
859 Geophysical   Research: Atmospheres,   126,   e2021JD035273,
860 https://doi.org/10.1029/2021JD035273, 2021.
861 Dai, T., Dai, Q., Ding, J., Liu, B., Bi, X., Wu, J., Zhang, Y., and Feng, Y.: Measuring the Emission
862 Changes and Meteorological Dependence of Source-Specific BC Aerosol Using Factor Analysis
863 Coupled With Machine Learning, Journal of Geophysical Research: Atmospheres, 128,
864 e2023JD038696, https://doi.org/10.1029/2023JD038696, 2023.
865 Ding, A. J., Huang, X., Nie, W., Sun, J. N., Kerminen, V.-M., Petäjä, T., Su, H., Cheng, Y. F., Yang, X.-
866 Q., Wang, M. H., Chi, X. G., Wang, J. P., Virkkula, A., Guo, W. D., Yuan, J., Wang, S. Y., Zhang, R. J.,
867 Wu, Y. F., Song, Y., Zhu, T., Zilitinkevich, S., Kulmala, M., and Fu, C. B.: Enhanced haze pollution by
868 black carbon in megacities in China, Geophysical Research Letters, 43, 2873-2879,
869 https://doi.org/10.1002/2016GL067745, 2016.
870 Ding, S., Zhao, D., Tian, P., and Huang, M.: Source apportionment and wet scavenging ability of
871 atmospheric black carbon during haze in Northeast China, Environmental Pollution, 357, 124470,
872 https://doi.org/10.1016/j.envpol.2024.124470, 2024.
873 Ding, S., Liu, D., Zhao, D., Tian, P., Huang, M., and Ding, D.: Characteristics of atmospheric black
874 carbon and its wet scavenging in Nanning, South China, Science of The Total Environment, 904,
875 166747, https://doi.org/10.1016/j.scitotenv.2023.166747, 2023.
876 Drinovec, L., Močnik, G., Zotter, P., Prévôt, A. S. H., Ruckstuhl, C., Coz, E., Rupakheti, M., Sciare, J.,
877 Müller, T., Wiedensohler, A., and Hansen, A. D. A.: The "dual-spot" Aethalometer: an improved
878 measurement of aerosol black carbon with real-time loading compensation, Atmos. Meas. Tech.,
879 8, 1965-1979, 10.5194/amt-8-1965-2015, 2015.
880 Du, H., Li, J., Wang, Z., Chen, X., Yang, W., Sun, Y., Xin, J., Pan, X., Wang, W., Ye, Q., and Dao, X.:
881 Assessment of the effect of meteorological and emission variations on winter PM2.5 over the North
882 China Plain in the three-year action plan against air pollution in 2018–2020, Atmospheric Research,
883 280, 106395, https://doi.org/10.1016/j.atmosres.2022.106395, 2022.
884 Dumka, U. C., Kaskaoutis, D. G., Devara, P. C. S., Kumar, R., Kumar, S., Tiwari, S., Gerasopoulos, E.,
885 and Mihalopoulos, N.: Year-long variability of the fossil fuel and wood burning black carbon
886 components at a rural site in southern Delhi outskirts, Atmospheric Research, 216, 11-25,
887 https://doi.org/10.1016/j.atmosres.2018.09.016, 2019.
888 Fan, M.-Y., Hong, Y., Zhang, Y.-L., Sha, T., Lin, Y.-C., Cao, F., and Guo, H.: Increasing Nonfossil Fuel

889 Contributions to Atmospheric Nitrate in Urban China from Observation to Prediction,
890 Environmental Science & Technology, 57, 18172-18182, 10.1021/acs.est.3c01651, 2023.

891 Fuller, G. W., Tremper, A. H., Baker, T. D., Yttri, K. E., and Butterfield, D.: Contribution of wood
892 burning to PM10 in London, Atmospheric Environment, 87, 87-94,
893 https://doi.org/10.1016/j.atmosenv.2013.12.037, 2014.

894 Grange, S. K., Carslaw, D. C., Lewis, A. C., Boleti, E., and Hueglin, C.: Random forest meteorological
895 normalisation models for Swiss PM10 trend analysis, Atmos. Chem. Phys., 18, 6223-6239,
896 10.5194/acp-18-6223-2018, 2018.

897 Gul, C., Mahapatra, P. S., Kang, S., Singh, P. K., Wu, X., He, C., Kumar, R., Rai, M., Xu, Y., and Puppala,
898 S. P.: Black carbon concentration in the central Himalayas: Impact on glacier melt and potential
899 source contribution, Environmental Pollution, 275, 116544,
900 https://doi.org/10.1016/j.envpol.2021.116544, 2021.

901 He, C., Niu, X., Ye, Z., Wu, Q., Liu, L., Zhao, Y., Ni, J., Li, B., and Jin, J.: Black carbon pollution in China
902 from 2001 to 2019: Patterns, trends, and drivers, Environmental Pollution, 324, 121381,
903 https://doi.org/10.1016/j.envpol.2023.121381, 2023.

904 Helin, A., Niemi, J. V., Virkkula, A., Pirjola, L., Teinilä, K., Backman, J., Aurela, M., Saarikoski, S., Rönkkö,
905 T., Asmi, E., and Timonen, H.: Characteristics and source apportionment of black carbon in the
906 Helsinki metropolitan area, Finland, Atmospheric Environment, 190, 87-98,
907 https://doi.org/10.1016/j.atmosenv.2018.07.022, 2018.

908 Hong, Y., Zhang, Y., Bao, M., Fan, M., Lin, Y. C., Xu, R., Shu, Z., Wu, J. Y., Cao, F., Jiang, H., Cheng,
909 Z., Li, J., and Zhang, G.: Nitrogen-Containing Functional Groups Dominate the Molecular
910 Absorption of Water-Soluble Humic-Like Substances in Air From Nanjing, China Revealed by the
911 Machine Learning Combined FT-ICR-MS Technique, Journal of Geophysical Research:
912 Atmospheres, 128, 10.1029/2023JD039459, 2023.

913 Huang, Z.-J., Li, H., Luo, J.-Y., Li, S., and Liu, F.: Few-Shot Learning-Based, Long-Term Stable,
914 Sensitive Chemosensor for On-Site Colorimetric Detection of Cr(VI), Analytical Chemistry, 95,
915 6156-6162, 10.1021/acs.analchem.3c00604, 2023.

916 IPCC: Climate Change 2022 – Impacts, Adaptation and Vulnerability: Working Group II
917 Contribution to the Sixth Assessment Report of the Intergovernmental Panel on Climate Change,
918 Cambridge University Press, Cambridge, 10.1017/9781009325844, 2023.

919 Jing, A., Zhu, B., Wang, H., Yu, X., An, J., and Kang, H.: Source apportionment of black carbon in
920 different seasons in the northern suburb of Nanjing, China, Atmospheric Environment, 201, 190-
921 200, https://doi.org/10.1016/j.atmosenv.2018.12.060, 2019.

922 Lee, B. P., Louie, P. K. K., Luk, C., and Chan, C. K.: Evaluation of traffic exhaust contributions to
923 ambient carbonaceous submicron particulate matter in an urban roadside environment in Hong
924 Kong, Atmos. Chem. Phys., 17, 15121-15135, 10.5194/acp-17-15121-2017, 2017.

925 Li, L., Li, Q., Huang, L., Wang, Q., Zhu, A., Xu, J., Liu, Z., Li, H., Shi, L., Li, R., Azari, M., Wang, Y.,
926 Zhang, X., Liu, Z., Zhu, Y., Zhang, K., Xue, S., Ooi, M. C. G., Zhang, D., and Chan, A.: Air quality
927 changes during the COVID-19 lockdown over the Yangtze River Delta Region: An insight into the
928 impact of human activity pattern changes on air pollution variation, Science of The Total
929 Environment, 732, 139282, https://doi.org/10.1016/j.scitotenv.2020.139282, 2020.

930 Li, R., Han, Y., Wang, L., Shang, Y., and Chen, Y.: Differences in oxidative potential of black carbon
931 from three combustion emission sources in China, Journal of Environmental Management, 240,

57-65, https://doi.org/10.1016/j.jenvman.2019.03.070, 2019.

Li, W., Liu, X., Duan, F., Qu, Y., and An, J.: A one-year study on black carbon in urban Beijing: Concentrations, sources and implications on visibility, Atmospheric Pollution Research, 13, 101307, https://doi.org/10.1016/j.apr.2021.101307, 2022.

Li, Y., Lei, L., Sun, J., Gao, Y., Wang, P., Wang, S., Zhang, Z., Du, A., Li, Z., Wang, Z., Kim, J. Y., Kim, H., Zhang, H., and Sun, Y.: Significant Reductions in Secondary Aerosols after the Three-Year Action Plan in Beijing Summer, Environmental Science & Technology, 57, 15945-15955, 10.1021/acs.est.3c02417, 2023.

Lin, Y.-C., Zhang, Y.-L., Xie, F., Fan, M.-Y., and Liu, X.: Substantial decreases of light absorption, concentrations and relative contributions of fossil fuel to light-absorbing carbonaceous aerosols attributed to the COVID-19 lockdown in east China, Environmental Pollution, 275, 116615, https://doi.org/10.1016/j.envpol.2021.116615, 2021.

Liu, D., He, C., Schwarz, J. P., and Wang, X.: Lifecycle of light-absorbing carbonaceous aerosols in the atmosphere, npj Climate and Atmospheric Science, 3, 40, 10.1038/s41612-020-00145-8, 2020a.

Liu, D., Ding, S., Zhao, D., Hu, K., Yu, C., Hu, D., Wu, Y., Zhou, C., Tian, P., Liu, Q., Wu, Y., Zhang, J., Kong, S., Huang, M., and Ding, D.: Black Carbon Emission and Wet Scavenging From Surface to the Top of Boundary Layer Over Beijing Region, Journal of Geophysical Research: Atmospheres, 125, e2020JD033096, https://doi.org/10.1029/2020JD033096, 2020b.

Liu, Y., Yan, C., and Zheng, M.: Source apportionment of black carbon during winter in Beijing, Science of The Total Environment, 618, 531-541, https://doi.org/10.1016/j.scitotenv.2017.11.053, 2018.

Lundberg, S. M. and Lee, S.-I.: A unified approach to interpreting model predictions, Advances in neural information processing systems, 30, 2017.

Qin, Y., Ye, J., Ohno, P., Liu, P., Wang, J., Fu, P., Zhou, L., Li, Y. J., Martin, S. T., and Chan, C. K.: Assessing the Nonlinear Effect of Atmospheric Variables on Primary and Oxygenated Organic Aerosol Concentration Using Machine Learning, ACS Earth and Space Chemistry, 6, 1059-1066, 10.1021/acsearthspacechem.1c00443, 2022.

Ramanathan, V. and Carmichael, G.: Global and regional climate changes due to black carbon, Nature Geoscience, 1, 221-227, 10.1038/ngeo156, 2008.

Ran, L., Deng, Z. Z., Wang, P. C., and Xia, X. A.: Black carbon and wavelength-dependent aerosol absorption in the North China Plain based on two-year aethalometer measurements, Atmospheric Environment, 142, 132-144, https://doi.org/10.1016/j.atmosenv.2016.07.014, 2016.

Sandradewi, J., Prévôt, A. S. H., Szidat, S., Perron, N., Alfarra, M. R., Lanz, V. A., Weingartner, E., and Baltensperger, U.: Using Aerosol Light Absorption Measurements for the Quantitative Determination of Wood Burning and Traffic Emission Contributions to Particulate Matter, Environmental Science & Technology, 42, 3316-3323, 10.1021/es702253m, 2008.

Sarigiannis, D., Karakitsios, S. P., Zikopoulos, D., Nikolaki, S., and Kermenidou, M.: Lung cancer risk from PAHs emitted from biomass combustion, Environ Res, 137, 147-156, 10.1016/j.envres.2014.12.009, 2015.

Seo, J., Park, D. S. R., Kim, J. Y., Youn, D., Lim, Y. B., and Kim, Y.: Effects of meteorology and emissions on urban air quality: a quantitative statistical approach to long-term records (1999–2016) in Seoul, South Korea, Atmos. Chem. Phys., 18, 16121-16137, 10.5194/acp-18-16121-2018, 2018.

975 Sun, J., Wang, Z., Zhou, W., Xie, C., Wu, C., Chen, C., Han, T., Wang, Q., Li, Z., Li, J., Fu, P., Wang, Z.,
976 and Sun, Y.: Measurement report: Long-term changes in black carbon and aerosol optical
977 properties from 2012 to 2020 in Beijing, China, Atmos. Chem. Phys., 22, 561-575, 10.5194/acp-
978 22-561-2022, 2022a.
979 Sun, X., Zhao, T., Bai, Y., Kong, S., Zheng, H., Hu, W., Ma, X., and Xiong, J.: Meteorology impact on
980 PM2.5 change over a receptor region in the regional transport of air pollutants: observational
981 study of recent emission reductions in central China, Atmos. Chem. Phys., 22, 3579-3593,
982 10.5194/acp-22-3579-2022, 2022b.
983 Wang, Y., Yuan, Y., Wang, Q., Liu, C., Zhi, Q., and Cao, J.: Changes in air quality related to the
984 control of coronavirus in China: Implications for traffic and industrial emissions, Science of The
985 Total Environment, 731, 139133, https://doi.org/10.1016/j.scitotenv.2020.139133, 2020.
986 Wei, C., Wang, M. H., Fu, Q. Y., Dai, C., Huang, R., and Bao, Q.: Temporal Characteristics and
987 Potential Sources of Black Carbon in Megacity Shanghai, China, Journal of Geophysical Research:
988 Atmospheres, 125, e2019JD031827, https://doi.org/10.1029/2019JD031827, 2020.
989 Wise, E. K. and Comrie, A. C.: Extending the Kolmogorov–Zurbenko Filter: Application to Ozone,
990 Particulate Matter, and Meteorological Trends, Journal of the Air & Waste Management
991 Association, 55, 1208-1216, 10.1080/10473289.2005.10464718, 2005.
992 Wu, B., Wu, C., Ye, Y., Pei, C., Deng, T., Li, Y. J., Lu, X., Wang, L., Hu, B., Li, M., and Wu, D.: Long-
993 term hourly air quality data bridging of neighboring sites using automated machine learning: A
994 case study in the Greater Bay area of China, Atmospheric Environment, 321, 120347,
995 https://doi.org/10.1016/j.atmosenv.2024.120347, 2024.
996 Xiao, S., Yu, X., Zhu, B., Kumar, K. R., Li, M., and Li, L.: Characterization and source apportionment
997 of black carbon aerosol in the Nanjing Jiangbei New Area based on two years of measurements
998 from Aethalometer, Journal of Aerosol Science, 139, 105461,
999 https://doi.org/10.1016/j.jaerosci.2019.105461, 2020.
1000 Yao, X., Chan, C. K., Fang, M., Cadle, S., Chan, T., Mulawa, P., He, K., and Ye, B.: The water-soluble
1001 ionic composition of PM2.5 in Shanghai and Beijing, China, Atmospheric Environment, 36, 4223-
1002 4234, https://doi.org/10.1016/S1352-2310(02)00342-4, 2002.
1003 Yin, C., Deng, X., Zou, Y., Solmon, F., Li, F., and Deng, T.: Trend analysis of surface ozone at
1004 suburban Guangzhou, China, Science of The Total Environment, 695, 133880,
1005 https://doi.org/10.1016/j.scitotenv.2019.133880, 2019.
1006 Yu, M., Zhang, Y.-L., Xie, T., Song, W., Lin, Y.-C., Zhang, Y., Cao, F., Yang, C., and Szidat, S.:
1007 Quantification of fossil and non-fossil sources to the reduction of carbonaceous aerosols in the
1008 Yangtze River Delta, China: Insights from radiocarbon analysis during 2014–2019, Atmospheric
1009 Environment, 292, 119421, https://doi.org/10.1016/j.atmosenv.2022.119421, 2023.
1010 Zhang, L., Shen, F., Gao, J., Cui, S., Yue, H., Wang, J., Chen, M., and Ge, X.: Characteristics and
1011 potential sources of black carbon particles in suburban Nanjing, China, Atmospheric Pollution
1012 Research, 11, 981-991, https://doi.org/10.1016/j.apr.2020.02.011, 2020.
1013 Zhang, Q., Streets, D. G., Carmichael, G. R., He, K. B., Huo, H., Kannari, A., Klimont, Z., Park, I. S.,
1014 Reddy, S., Fu, J. S., Chen, D., Duan, L., Lei, Y., Wang, L. T., and Yao, Z. L.: Asian emissions in 2006
1015 for the NASA INTEX-B mission, Atmos. Chem. Phys., 9, 5131-5153, 10.5194/acp-9-5131-2009,
1016 2009.
1017 Zhang, Q., Zheng, Y., Tong, D., Shao, M., Wang, S., Zhang, Y., Xu, X., Wang, J., He, H., Liu, W., Ding,

Y., Lei, Y., Li, J., Wang, Z., Zhang, X., Wang, Y., Cheng, J., Liu, Y., Shi, Q., Yan, L., Geng, G., Hong, C., Li, M., Liu, F., Zheng, B., Cao, J., Ding, A., Gao, J., Fu, Q., Huo, J., Liu, B., Liu, Z., Yang, F., He, K., and Hao, J.: Drivers of improved PM$_{2.5}$ air quality in China from 2013 to 2017, Proceedings of the National Academy of Sciences, 116, 24463-24469, doi:10.1073/pnas.1907956116, 2019.

Zhang, X., Rao, R., Huang, Y., Mao, M., Berg, M. J., and Sun, W.: Black carbon aerosols in urban central China, Journal of Quantitative Spectroscopy and Radiative Transfer, 150, 3-11, https://doi.org/10.1016/j.jqsrt.2014.03.006, 2015.

Zhang, Y.-L., Li, J., Zhang, G., Zotter, P., Huang, R.-J., Tang, J.-H., Wacker, L., Prévôt, A. S. H., and Szidat, S.: Radiocarbon-Based Source Apportionment of Carbonaceous Aerosols at a Regional Background Site on Hainan Island, South China, Environmental Science & Technology, 48, 2651-2659, 10.1021/es4050852, 2014.

Zhao, C., Wang, Q., Ban, J., Liu, Z., Zhang, Y., Ma, R., Li, S., and Li, T.: Estimating the daily PM2.5 concentration in the Beijing-Tianjin-Hebei region using a random forest model with a 0.01° × 0.01° spatial resolution, Environment International, 134, 105297, https://doi.org/10.1016/j.envint.2019.105297, 2020.

Zheng, H., Kong, S., Zhai, S., Sun, X., Cheng, Y., Yao, L., Song, C., Zheng, Z., Shi, Z., and Harrison, R. M.: An intercomparison of weather normalization of PM2.5 concentration using traditional statistical methods, machine learning, and chemistry transport models, npj Climate and Atmospheric Science, 6, 214, 10.1038/s41612-023-00536-7, 2023.

Zheng, H., Kong, S. F., Zheng, M. M., Yan, Y., Yao, L., Zheng, S., Yan, Q., Wu, J., Cheng, Y., Chen, N., Bai, Y., Zhao, T., Liu, D., Zhao, D., and Qi, S.: A 5.5-year observations of black carbon aerosol at a megacity in Central China: Levels, sources, and variation trends, Atmospheric Environment, 232, 117581, https://doi.org/10.1016/j.atmosenv.2020.117581, 2020.

Zhou, B., Wang, Q., Zhou, Q., Zhang, Z., Wang, G., Fang, N., Li, M., and Cao, J.: Seasonal Characteristics of Black Carbon Aerosol and its Potential Source Regions in Baoji, China, Aerosol and Air Quality Research, 18, 397-406, 10.4209/aaqr.2017.02.0070, 2018.

Zhou, Y., Ma, X., Tian, R., and Wang, K.: Seasonal transition of Black carbon aerosols over Qinghai-Tibet Plateau: Simulations with WRF-Chem, Atmospheric Environment, 308, 119866, https://doi.org/10.1016/j.atmosenv.2023.119866, 2023.

Zhu, C., Kanaya, Y., Takigawa, M., Ikeda, K., Tanimoto, H., Taketani, F., Miyakawa, T., Kobayashi, H., and Pisso, I.: FLEXPART v10.1 simulation of source contributions to Arctic black carbon, Atmos. Chem. Phys., 20, 1641-1656, 10.5194/acp-20-1641-2020, 2020.

Zhuang, B. L., Wang, T. J., Liu, J., Li, S., Xie, M., Yang, X. Q., Fu, C. B., Sun, J. N., Yin, C. Q., Liao, J. B., Zhu, J. L., and Zhang, Y.: Continuous measurement of black carbon aerosol in urban Nanjing of Yangtze River Delta, China, Atmospheric Environment, 89, 415-424, https://doi.org/10.1016/j.atmosenv.2014.02.052, 2014.

Zong, Z., Wang, X., Tian, C., Chen, Y., Qu, L., Ji, L., Zhi, G., Li, J., and Zhang, G.: Source apportionment of PM2.5 at a regional background site in North China using PMF linked with radiocarbon analysis: insight into the contribution of biomass burning, Atmos. Chem. Phys., 16, 11249-11265, 10.5194/acp-16-11249-2016, 2016.

Zotter, P., Herich, H., Gysel, M., El-Haddad, I., Zhang, Y., Močnik, G., Hüglin, C., Baltensperger, U., Szidat, S., and Prévôt, A. S. H.: Evaluation of the absorption Ångström exponents for traffic and

1061 wood burning in the Aethalometer-based source apportionment using radiocarbon
1062 measurements of ambient aerosol, Atmos. Chem. Phys., 17, 4229-4249, 10.5194/acp-17-4229-
1063 2017, 2017.
1064